A Beamforming Aided Full-Diversity Scheme for Low-Altitude Air-to-Ground Communication Systems Operating with Limited Feedback

Rakshith Rajashekar, *Senior Member, IEEE*, Marco Di Renzo, *Senior Member, IEEE*, K.V.S. Hari, *Fellow, IEEE* and L. Hanzo, *Fellow, IEEE*

***Abstract*—Unmanned aerial vehicles (UAV) have gained significant popularity in the recent past owing to their easy deployability and wide range of applications. In most of the short and medium range applications, WiFi is used as the access technology for establishing communication between the ground stations and the UAVs. Although WiFi is known to perform well in most of the scenarios, it is important to note that WiFi has been mainly designed for indoor communication in rich scattering environments, whereas the air-to-ground (A2G) channel is characterised by sparse scattering. Considering this important difference in the channel characteristics, we revisit some of the WiFi features and propose efficient design alternatives. Firstly, we provide a statistical model for the sparse A2G channel and design an optimal time-domain quantizer (TDQ) for its feedback. In contrast to the frequency-domain quantizer (FDQ) of 802.11n/ac standard, the proposed TDQ exploits the time-domain sparsity in the channel and requires about fifteen times lesser quantization bits than FDQ. Secondly, we propose a beamforming scheme with the aid of full-diversity rotation (FDR) matrices and analytically evaluate its symbol error probability in order to quantify the attainable diversity order. Our numerical simulations demonstrate that the proposed FDR beamforming (FDR-BF) scheme outperforms the relevant benchmark schemes in both coded as well as uncoded scenarios. Specifically, the proposed FDR-BF scheme was observed to attain a signal-to-noise ratio gain as high as 6dB compared to the popular geometric mean decomposition based beamforming scheme, when operating at an elevation angle of 7.5^o.**

***Index Terms*—Low-altitude platforms, drones, beamforming, time-domain quantization, and 802.11.**

I. Introduction

The future wireless infrastructure is envisaged to grow beyond the terrestrial realm owing to the rapid proliferation of easily deployable unmanned aerial vehicles (UAV), such as drones, tethered helikites, mini aircrafts etc. [1]-[4]. Among these UAVs, drones have gained significant popularity owing to their wide range of applications such as video surveillance, mapping, safe inspection of power lines/cell towers, search and rescue operations, crop-surveying etc. In the event of a disaster, a robust and reliable network, which can be promptly deployed, becomes necessary for aiding the disaster management operations as well as for providing temporary coverage over the disaster-struck region. Drones deployed as low-altitude platforms (LAPs)[1] [5] that provide connectivity via wireless fidelity (WiFi), or worldwide interoperability for microwave access (WiMAX) and terrestrial trunked radio (TETRA) were experimentally studied in [6], while that relying on long term evolution-advanced (LTE-A) was studied in [7]. Adaptive modulation and coding was designed in [8]. Among these diverse wireless access technologies, WiFi has gained a significant popularity among drones [9]-[14] owing to its ubiquity and versatile *infrastructure* based and *ad-hoc* modes of operation, which are sufficient to cater for a wide range of applications. Specifically, Zhiqiang *et al.* studied the robustness of IEEE 802.11a in the presence of high doppler shifts [9], while Evsen *et al.* studied the impact of both the 3D dynamics and of the orientation of the UAVs on the performance of an 802.11a network [10]. In [11], Mahadi *et al.* have evaluated the impact of a) both the distance and of the relative speed between the UAVs; b) the orientation of the antennas and the trajectory of the UAVs; c) the energy efficiency and the data rate, on the performance of an 802.11n network. In [12], Evsen *et al.* have studied the performance of the infrastructure and mesh modes of 802.11a, both in single and dual-hop communication scenarios. By contrast, Samera *et al.* have studied the performance of multi-UAV aided communication in 802.11a and 802.11ac networks [13]. In [14], Antonio *et al.* have studied the performance of both infrastructure-based and ad-hoc modes of 802.11 in terms of throughput, coverage area and energy efficiency. In [15], Jamal *et al.* investigated multiple antenna and diversity techniques in multicarrier communication systems and showed that receive antenna separation increases the diversity gain of the system at short link distances. In [16], Zhang *et al.* studied the adaptive MIMO antenna array where the antenna spacing was optimized to reduce the channel correlation and maximize the system capacity. In [17], Chen *et al.* implemented and

R. Rajashekar and L. Hanzo are with the School of ECS, University of Southampton, SO17 1BJ, UK (e-mail: rmr1u14@soton.ac.uk, lh@ecs.soton.ac.uk).

K.V.S. Hari is with the Dept. of ECE, Indian Institute of Science, Bangalore, 560012, India (e-mail: hari@ece.iisc.ernet.in).

M. Di Renzo is with the Laboratoire des Signaux et Systèmes, CNRS, CentraleSupélec, Univ Paris Sud, Université Paris-Saclay, 3 rue Joliot Curie, Plateau du Moulon, 91192 Gif-sur-Yvette, France. (e-mail: marco.direnzo@l2s.centralesupelec.fr). His work is supported in part by the Agence Nationale de la Recherche Scientifique (ANR) through the research project SpatialModulation (Société de l'Information et de la Communication – Action Plan 2015).

The financial support of the EPSRC projects EP/P034284/1, EP/N004558/1 and EP/L018659/1, as well as of the Royal Society's Wolfson Research Merit Award is gratefully acknowledged.

[1]LAPs are deployed in the lower troposphere, where as high altitude platforms (HAP) are deployed in the stratosphere.

studied the performance of a long-range broadband aerial communication system using directional antennas.

The classic singular value decomposition (SVD) based beamforming [18] yields parallel sub-channels with unequal signal-to-noise ratios (SNR). The optimal water-filling power allocation [18] would simply assign zero power to some of the low-SNR parallel sub-channels. This would require non-uniform bit-loading, which is practically infeasible. When using uniform bit-loading across all the sub-channels, the effective bit error ratio (BER) performance will be dominated by the sub-channels having low SNRs. Some of the existing solutions that attempt to address this issue include the popular geometric mean decomposition (GMD) based beamforming [19], [20], the uniform channel decomposition (UCD) based beamforming [21], and the space-time block coding (STBC) aided beamforming schemes [22]-[26]. The GMD based beamforming provides identical SNRs across the subchannels, but does not provide any transmit diversity gain, while the UCD based beamforming overcomes this impediment, but at a high computational complexity. The STBC aided beamforming schemes attain the transmit diversity gain at the cost of multiplexing gain.

Although the extensive experimental studies of [9]-[14] confirm that WiFi may indeed be used in LAPs, several of its enhancements/features would be suboptimal in aerial communication scenarios, since its features were designed for indoor wireless channels, which are characterized by rich multipath scattering, whereas the air-to-ground (A2G) wireless channel is characterised by sparse multipath scattering [27]-[30]. Specifically, the delay spread of the indoor channel is not expected to vary significantly, whereas that of the air-to-ground channel may vary significantly, depending on the elevation of the UAV with respect to the ground station [27]. Furthermore, the A2G channel would have a strong line-of-sight (LoS) component, whereas the indoor channel will not have a LoS component in general. Thus, the features of 802.11 that are designed by taking into account the channel characteristics, such as the cyclic prefix (CP), channel quantization, beamforming etc. have to be revisited in the context of A2G communication.

Against this background, the contributions of this paper are as follows:

1) While the various channel measurements found in the literature [27]-[30] provide significant insight into the nature of the A2G channel, they cannot be readily utilized for system design and performance evaluation. A statistical channel model [31], which can be readily tuned for different aerial scenarios would be highly beneficial. In this paper, we first propose a simple statistical channel model and provide the specific model parameters that fit the A2G channel measurement data given in [27] for the elevation angles of $\Psi \in \{7.5^o, 15^o, 22.5^o, 30^o\}$. We use this channel model for designing the time-domain channel quantizer as well as for the performance evaluation of the proposed scheme.
2) One of the important features provided by the 802.11n/ac standard [32] is the beamforming[2] [33]-[36], which exploits the knowledge of channel state information (CSI) at the transmitter for improving the transmission range. A key requirement of beamforming is the availability of the CSI at the transmitter, which is accomplished by the frequency domain quantizer (FDQ) employed in 802.11n/ac (20.3.12.3.2 [32]). In contrast to this, motivated by the time-domain sparsity of the A2G channel (Sec. V, Sec. VI, and Sec. III-E in [27], [28], and [29] resp.), we propose a practically motivated time-domain quantizer (TDQ) [35], [37] that operates at the *rate-distortion limit* [38]. Furthermore, we show that the proposed TDQ would significantly reduce the feedback overhead involved in the beamforming, while attaining the same performance as that of FDQ.
3) In contrast to the existing beamforming schemes [19]-[26] discussed earlier, we propose a full-diversity rotation (FDR) [39]-[41] aided beamformer (FDR-BF) that attains the maximum achievable transmit diversity gain without compromising the multiplexing gain. Furthermore, the proposed scheme is shown to attain a significant performance gain over the existing schemes.

The remainder of the paper is organized as follows. The A2G statistical channel model as well as the proposed TDQ are presented in Section II-A and Section II-B, respectively. The proposed FDR based beamforming as well as its diversity analysis are presented in Section III. Our simulation results and discussions are provided in Section IV, while Section V concludes the paper.

Notations: A circularly symmetric complex-valued Gaussian distribution with mean μ and variance σ^2 is represented by $\mathcal{CN}(\mu, \sigma^2)$. An upper truncated Weibull distribution with shape parameter k, scale parameter λ and truncating point B is represented by $\mathcal{WB}(k, \lambda, B)$. The notations of $(\cdot)^H$ and $(\cdot)^T$ indicate the Hermitian transpose and transpose of a vector/matrix, respectively, while $|\cdot|$ represents the magnitude of a complex quantity, or the cardinality of a given set. The uppercase boldface letters represent matrices and lowercase boldface letters represent vectors. The notations of $\|\cdot\|_F$, $\|\cdot\|_0$ and $\|\cdot\|$ represent the Frobenious norm of a matrix, the l_0-norm of a vector and the l_2-norm of a vector, respectively. $\mathbf{H}([c:d],:)$ represents a matrix with rows $c, c+1, \ldots, d-1, d$ of $\mathbf{H}$ and $\mathbf{H}(:,[c:d])$ is a matrix with columns $c, c+1, \ldots, d-1, d$ of $\mathbf{H}$. The k^{th} element of a vector $\mathbf{s}$ is denoted by $\mathbf{s}(k)$. Expected value of a random variable Y is denoted by $\mathbb{E}(Y)$. Furthermore, $Q(x)$ represents the tail probability of standard normal distribution given by $\frac{1}{\sqrt{2\pi}} \int_x^\infty \exp\left(-\frac{u^2}{2}\right) du$. $\mathbb{C}$ and $\mathbb{R}$ represent the field of complex and real numbers, respectively.

II. Statistical A2G Channel Model and the Proposed Time-Domain Quantizer

In this section, we first present our statistical model of the A2G channel, which is based on the measurement data of

[2]Note that the 802.11 standard provides both implicit and explicit beamforming features (20.3.12.2 and 20.3.12.3 in [32]) resp.). Throughout this paper, we consider only the explicit beamforming with CSI matrices feedback as detailed in 20.3.12.3.2 in [32].

[27], followed by our proposed TDQ for the A2G channel, which imposes very low feedback overhead compared to the conventional FDQ [32].

A. Statistical A2G Channel Model

Let L_t denote the number of multipath components between the ground station and the aerial transmitter deployed as a LAP. Let α_i and τ_i denote the complex-valued gain and the delay associated with the i^{th} multipath component, respectively. The multipath channel is given by

$$h(\tau) = \sum_{i=0}^{L_t-1} \alpha_i \delta(\tau - \tau_i), \tag{1}$$

where we have $\alpha_i \sim \mathcal{CN}(0, \sigma_i^2)$, $\sigma_i = \Omega\beta^i$, $1 \leq i \leq L_t - 1$, $0 < \beta \leq 1$, $h(\tau)$ is the impulse response of the channel, $\delta(x) = 1$ if $x = 0$ and 0 otherwise. The normalization factor Ω is chosen so that $\Omega \sum_{i=0}^{L_t-1} \beta^i = 1$. Furthermore, α_0 is modeled as a Rician fading component with the ratio of power in the LoS component compared to that of non-LoS component denoted by K, i.e. $\alpha_0 \sim \sqrt{\frac{K}{1+K}}\sigma_0 + \sqrt{\frac{1}{1+K}}\mathcal{CN}(0, \sigma_0^2)$. The multipath delays are modeled by statistically independent truncated Weibull random variables, i.e. $\tau_i \sim \mathcal{WB}(k, \lambda, B)\ \forall i$.

It was observed in [27] (Section V) that the average number of paths in the LAP scenario is 7.88. Thus, we consider $L_t = 8$ for all the four elevation profiles in our model. Furthermore, considering a power margin of 25dB with respect to the strongest multipath component, the limits of the excess delay for elevation angles of $7.5^o, 15^o, 22.5^o, 30^o$ are given by 1550ns, 1480ns, 1294ns, 1290ns (Table 2, [27]), respectively. Thus, we consider $B \in \{1550, 1480, 1294, 1290\}$ for the four elevation profiles. Furthermore, the choice of $\lambda \in \{1000, 460, 205, 161\}$, $K(dB) \in \{0, 6, 12, 20\}$, $\beta \in \{0.27, 0.26, 0.26, 0.24\}$ and $k = 1.1$ for all the elevation profiles results in an average root mean squared (RMS) delay spread [18] similar to that of the measured data (refer to Table 1 in [27]). The RMS delay spread for a given channel realization is given by $\frac{\sum_i |\alpha_i|^2(\tau_i - \hat{\tau})^2}{\sum_i |\alpha_i|^2}$, where $\hat{\tau} = \frac{\sum_i \tau_i |\alpha_i|^2}{\sum_i |\alpha_i|^2}$, $0 \leq i \leq L_t - 1$ in all the summations. The parameters of the A2G channel model for various elevation angles are provided in Table I. The mean RMS delay spread recorded for the various elevation angles based on the measured data as well as that obtained by the channel model considered above are listed in Table II. It is evident from Table II that the mean RMS delay spread computed using the statistical channel model is quite close that of the measured data [27]. Furthermore, the complementary cumulative distribution function (CCDF) function of the RMS delay spread recorded for various elevation angles and computed based on the proposed statistical channel model is provided in Fig. 1. The CCDF of the RMS delay spread presented in Fig. 1 coincides with that of the measured data presented in Fig. 3 of [27]. Thus, we conclude from Table II and Fig. 1 that the proposed statistical channel model is a good approximation of the A2G multipath channel and hence can be utilized for system design and performance analysis[3].

TABLE I
MODEL PARAMETERS FOR THE PROPOSED STATISTICAL A2G CHANNEL MODEL.

Elevation angle (Ψ)	K-factor of the LoS path (dB)	Multipath delay parameters (k, λ, B)	Multipath variance parameter (β)
7.5^o	0	$(1.1, 1000, 1550)$	0.27
15^o	6	$(1.1, 460, 1480)$	0.26
22.5^o	12	$(1.1, 205, 1294)$	0.26
30^o	20	$(1.1, 161, 1290)$	0.24

TABLE II
COMPARISON OF THE MEAN RMS DELAY SPREAD - MEASURED DATA [27] VS. STATISTICAL CHANNEL MODEL.

Elevation angle (Ψ)	Mean RMS Delay Spread (ns) from **Measured Data [27]**	Mean RMS Delay Spread (ns) from **Statistical Model**
7.5^o	98.1	95.8
15^o	54.9	54.7
22.5^o	24.3	24.8
30^o	18.3	17.8

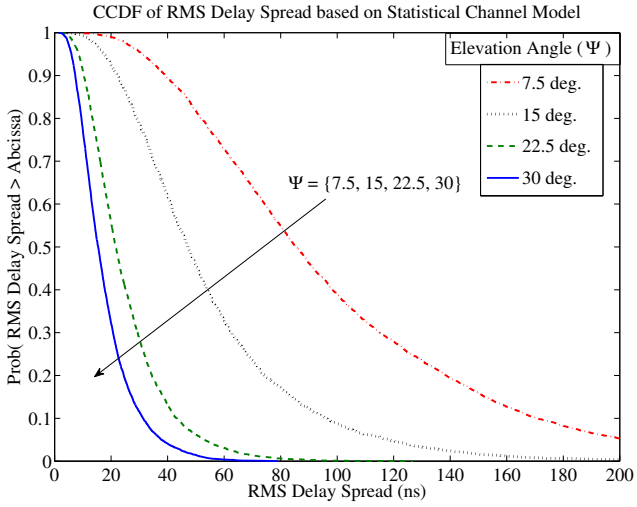

Fig. 1. The CCDF of RMS delay spread for elevation angles $\Psi \in \{7.5^o, 15^o, 22.5^o, 30^o\}$ computed based on the proposed statistical channel model.

B. Proposed TDQ for A2G channel

In MIMO-OFDM systems employing beamforming, CSI is required at the transmitter, which is attained by quantizing the channel at the receiver and sending the same to the transmitter. The 802.11n/ac (20.3.12.3.4 [32]) quantizes the channel in the frequency domain since the indoor channel exhibits rich scattering. However, in A2G link, the channel is sparse and hence offers very low-feedback overhead when quantized in the time domain. In the following we describe the TDQ and its implementation.

[3]Note that we have not considered the channel variation in time due to vehicle dynamics, since we are only interested in the case where the transmission frames do not exceed the channel coherence time.

TABLE III
OPTIMAL NUMBER OF QUANTIZATION BITS FOR VARIOUS DISTORTION LEVELS D_t AT THE ELEVATION ANGLE $\Psi = 7.5^o$.

Quant. bits	$D_t = 10^{-1}$	$D_t = 10^{-2}$	$D_t = 10^{-3}$	$D_t = 10^{-4}$
B_0	6	10	13	16
B_1	4	8	11	14
B_2	3	6	9	13
B_3	1	4	7	11
B_4	$*$	2	5	9
B_5	$*$	$*$	4	7
B_6	$*$	$*$	2	5
B_7	$*$	$*$	$*$	3
Total	14	30	51	78

Since the K-factor associated with α_0 may vary significantly depending on the elevation angle [27], we consider α_0 to be Gaussian distributed in order to cater for the worst-case scenario. In other words, the Gaussian assumption ensures that α_0 will have maximum number of quantization levels in order to meet the rate distortion limit. Let the multipath channel coefficients be denoted by $\boldsymbol{\alpha} = [\alpha_0, \alpha_1, \ldots, \alpha_{L_t-1}]^T$ and the quantized channel coefficients be denoted by $\boldsymbol{\alpha}^q = [\alpha_0^q, \alpha_1^q, \ldots, \alpha_{L_t-1}^q]^T$. If the total affordable mean-squared distortion is $D_t = \mathbb{E}\big[\|\boldsymbol{\alpha} - \boldsymbol{\alpha}^q\|^2\big]$, upon assuming uniform distortion across all the quantized taps, for the average distortion per quantized tap we have D_t/L_t. From *Theorem 13.3.2* of [38], the optimal number of quantization bits for the i^{th} multipath tap is given by

$$B_i = \left[\log_2\left(\frac{\sigma_i^2 L_t}{D_t}\right)\right]_+, \tag{2}$$

where $[x]_+ = \max(x, 0)$. Since it is widely recognized that a uniform scalar quantizer approaches the rate-distortion limit of a Gaussian source up to a constant gap [37], we exploit this for quantizing the real and imaginary parts of the multipath channel coefficients. Let $\bar{B}_i = \lceil \frac{B_i}{2} \rceil$ represent the number of bits available for quantizing the real and imaginary components of the i^{th} multipath coefficient. The quantization interval size is chosen to be [37]:

$$\Delta_i = \sqrt{\frac{4B_i\sigma_i^2}{\log_2 e}} 2^{-\bar{B}_i}, \tag{3}$$

where $e = 2.7183$. (3) ensures that the distortion (D_t/L_t) decays exponentially with $\bar{B}_i$ for each of the taps. The optimal number of quantization bits for different distortion levels in case of $\Psi = 7.5^o$ is provided in Table III. From Table III we see that as D_t reduces from 10^{-1} to 10^{-4}, the number of taps with non-zero bit allocations increases from 4 to 8. Similar observations hold for the other elevation angles as well.

Although the number of analog multipath components is fixed to $L_t = 8$, the number of paths in the digital baseband domain would vary due to the finite sampling resolution. For instance, if $1/W$ is the sampling period, where W is the signal bandwidth, then the paths that fall within the time interval $-1/2W$ to $1/2W$ from the sampling epoch cannot be resolved. Thus, the number L_a of sampled multipath components may not be known to the receiver *a priori*. Assuming a nominal sampling frequency of 20MHz, the digital baseband channel[4] is modeled as

$$h(l) = \sum_{i=0}^{L_a-1} \alpha_{p_i}\delta(l - m_i), \tag{4}$$

where $L_a \leq L_t$ and $0 \leq m_i \leq 31$, which corresponds to a delay of 0ns to 1600ns that caters for a wide range of delays associated with various elevation angles. Among the multipath taps that fall in the interval $j/W \leq \tau < (j+1)/W$ $(0 \leq j \leq 31)$, the one closest to the sampling epoch[5] (j/W) is considered to be the sampled tap.

Let $\bar{\boldsymbol{\alpha}} = [\alpha_{p_0}, \alpha_{p_1}, \ldots, \alpha_{p_{L_a-1}}]^T$ represent the set of L_a sampled taps, where $0 \leq p_0 < p_1 \cdots < p_{L_a-1} \leq L_t - 1$. Note that the receiver may not know the statistics associated with the sampled taps, since the tap-indices p_i are not known *a priori*. Hence, the receiver may not be able to choose the right quantization resolution for each of the sampled taps. This issue is overcome by employing a simple algorithm based on combinatorial search, whose details are given below.

Given that the affordable distortion limit is D_t, the associated maximum number of quantization taps with non-zero quantization bits is given by $L_q = \max\{i \mid 0 \leq i \leq L_t - 1, B_i > 0\} + 1$, and the associated quantizers be represented by $\mathcal{Q}_0, \mathcal{Q}_1, \cdots, \mathcal{Q}_{L_q-1}$, which employ $B_0, B_1, \ldots, B_{L_q-1}$ quantization bits, respectively. Given $I = \{i_0, i_1, \ldots, i_{|I|-1}\} \subseteq \{i\}_{i=0}^{L_q-1}$, we use the notation $\mathcal{Q}_I$ for representing $[\mathcal{Q}_{i_0}, \mathcal{Q}_{i_1}, \ldots, \mathcal{Q}_{i_{|I|-1}}]^T$. For any given $\mathbf{a} \in \mathbb{C}^{|I|}$, we have $\mathcal{Q}_I : \mathbf{a} \rightarrow \mathbf{a}^q$, where $\mathbf{a}^q(k) = \mathcal{Q}_{i_k}[\mathbf{a}(k)]$ for $0 \leq k \leq |I| - 1$.

Depending on the value of L_a, which in turn depends on the channel realization, two scenarios may arise: $L_q \leq L_a$ and $L_q > L_a$. When $L_q \leq L_a$, the first L_q out of the L_a taps are quantized. When $L_q > L_a$, we have to search for the appropriate quantization taps that minimize the effective distortion. Let the enumerations of $n = \binom{L_q}{L_a}$ possible combinations be represented by $\{I_i\}_{i=1}^n$, where the elements in each of I_i are assumed to be in ascending order. Let $\mathcal{Q}_{I_j}$ represent the quantizer that considers the quantization taps to be those given by the set I_j. The effective distortion associated with the choice of I_j is $d_j = \|\bar{\boldsymbol{\alpha}} - \mathcal{Q}_{I_j}(\bar{\boldsymbol{\alpha}})\|^2$. The optimal set of quantization taps is the one that provides the least distortion, i.e. $I^* = I_{j^*}$, where $j^* = \arg\min_i d_i$. Algorithm 1 outlines the above combinatorial search.

Fig. 2 compares the average empirical distortion for various elevation angles as a function of the number quantization bits. It is evident from Fig. 2 that for $\Psi = 7.5^o$ the average distortion varies approximately from 10^{-1} to 10^{-4}, as the number of quantization bits is increased from 14 to 78 (refer to Table III), which validates the optimality of the number of quantization bits given in (2) as well as the efficiency of Algorithm 1. Similar observations hold for other elevation

[4]Considering a sampling frequency of 20MHz and the time-domain sparsity of the A2G channel, the digital baseband channel given in (4) is a fair approximation. When the sampling frequency is high, the effect of transmit and receive front-end filters become prominent and hence should be taken into account.

[5]Sampling epoch is the time instant at which the analog signal is digitized by the analog-to-digital converter (ADC) at the receiver.

Algorithm 1 Combinatorial Search for Optimal TDQ Taps.

Require: $\bar{\boldsymbol{\alpha}}$, L_a, L_q, $n = \binom{L_q}{L_a}$, and $\{I_i\}_{i=1}^{n}$.
  if $L_q \leq L_a$ **then**
    $I^* = [0, 1, \ldots, L_q - 1]$.
  else
    for $i = 1 : n$ **do**
      $d_i = \|\bar{\boldsymbol{\alpha}} - \mathcal{Q}_{I_i}(\bar{\boldsymbol{\alpha}})\|^2$.
    end for
    $j^* = \arg\min_i d_i$,
    $I^* = I_{j^*}$.
  end if

angles as well.

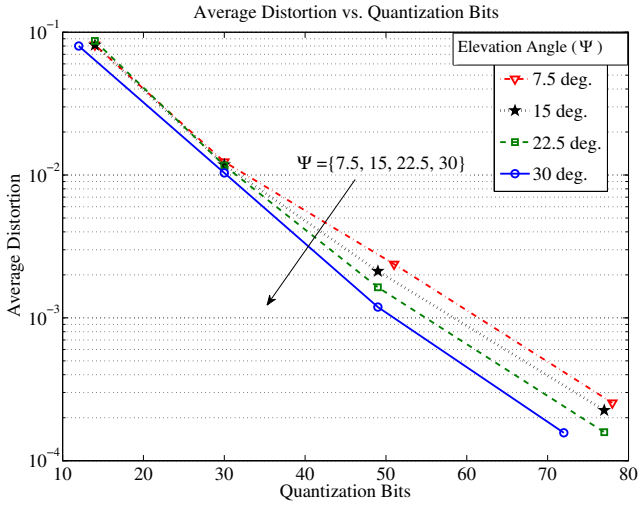

Fig. 2. Empirical average distortion as a function of quantization bits for various elevation angles. The average distortion is computed by considering thousand independent channel realizations for each of the elevation angles.

Proposed TDQ vs. FDQ of 802.11 [32]: We will show in Section IV that a distortion level of 10^{-2} would be sufficient to attain nearly the same BER performance as that attained with the aid of perfect CSI, and hence 30 bits would be sufficient[6] to quantize each of the links between the transmit and receive antenna pair. That is, a total of $N_{TDQ} = 30N_tN_r$ bits are required in case of the proposed TDQ, where N_t and N_r are the number of transmit and receive antennas, respectively. By contrast, the FDQ of 802.11n/ac would require $N_{FDQ} = (3 + 2N_cN_rN_b)N$ bits (20.3.12.3.4 [32]), where N is the number of subcarriers, $N_b \in \{4, 5, 6, 8\}$ is the number of quantization bits and N_c is the number of transmit streams. Note that N_{FDQ} scales with N, whereas N_{TDQ} does not. For instance, with a bandwidth of $W = 20$MHz, we have $N = 52$ data subcarriers. With $N_t = N_r = 2 = N_c$ and $N_b = 4$, we have $N_{FDQ} = 1820$ bits. Finally, for the same system configuration, we have $N_{TDQ} = 120$ bits, which is about fifteen times lower than N_{FDQ}.

[6]Note that the knowledge of delays (m_i) will be available at the transmitter due to channel reciprocity and hence need not be explicitly conveyed.

III. Proposed Full Diversity Rotation aided Beamforming Scheme

In this section, we first present the system model of the MIMO-OFDM in the time and frequency domains, followed by the proposed FDR-BF scheme which attains the full diversity gain without compromising on the spatial multiplexing gain.

A. System Model

Consider a multiple-input multiple-output (MIMO) aerial communication system having N_t transmit and N_r receive antennas, where the transmitter is carried by a LAP, while the receiver is assumed to be at a fixed location on ground. Let N represent the number of data subcarriers, $N_{SS} = \min(N_t, N_r)$ represent the number of spatial streams and N_{CP} represent the length of CP in terms of the number of samples. Let $\mathbf{F}_N \in \mathbb{C}^{N\times N}$ and $\mathbf{F}_N^{\dagger} = \mathbf{F}_N^H/N \in \mathbb{C}^{N\times N}$ represent the discrete Fourier transform (DFT) and inverse DFT matrices [18], respectively, i.e. $\{\mathbf{F}_N\}_{m,n} = e^{-j2\pi(m-1)(n-1)/N}$ for $1 \leq m, n \leq N$. The channel between each of the transmit and receive antenna pairs is modeled as a sparse multipath channel given by (4). Specifically, the channel between the i^{th} receive and the j^{th} transmit antenna is denoted by $\mathbf{h}_{ij} \in \mathbb{C}^{N_{CP}}$ and its frequency-domain representation is given by $\mathbf{h}'_{ij} = \mathbf{F}_N[\mathbf{h}_{ij}^T, \mathbf{0}^T]^T \in \mathbb{C}^N$. Considering orthogonal frequency division multiplexing (OFDM) based transmission [18] with perfect time and frequency synchronization, the received baseband signal at the i^{th} receive antenna after the removal of CP is given by

$$\mathbf{y}_i = \sum_{j=1}^{N_t} \mathbf{H}_{ij}\mathbf{x}_j + \mathbf{n}_i \quad \forall\ 1 \leq i \leq N_r, \tag{5}$$

where $\mathbf{H}_{ij} \in \mathbb{C}^{N\times N}$ represents the circulant matrix corresponding to the channel between the i^{th} receive and the j^{th} transmit antenna. Furthermore, $\mathbf{x}_j \in \mathbb{C}^N$ represents the OFDM symbol in the time-domain transmitted from the j^{th} transmit antenna, while the elements of $\mathbf{n}_i \in \mathbb{C}^N$ are from $\mathcal{CN}(0, \sigma_n^2)$, where σ_n^2 is the noise variance. The signal received at the i^{th} antenna in the frequency-domain is given by

$$\mathbf{y}'_i = \mathbf{F}_N\mathbf{y}_i = \sum_{j=1}^{N_t} \mathbf{F}_N\mathbf{H}_{ij}\mathbf{F}_N^{\dagger}\mathbf{x}'_j + \mathbf{F}_N\mathbf{n}_i, \tag{6}$$

$$= \sum_{j=1}^{N_t} \mathbf{\Lambda}_{ij}\mathbf{x}'_j + \mathbf{n}'_i, \tag{7}$$

where $\mathbf{\Lambda}_{ij} \in \mathbb{C}^{N\times N}$ is the diagonal matrix with $\mathbf{\Lambda}_{ij}(k,k) = \mathbf{h}'_{ij}(k)$ for $1 \leq k \leq N$, while $\mathbf{x}'_j \in \mathbb{C}^N$ represents the frequency-domain symbols transmitted from the j^{th} transmit antenna. The signal received at the k^{th} subcarrier is given by

$$\bar{\mathbf{y}}_k = \bar{\mathbf{H}}_k\bar{\mathbf{x}}_k + \bar{\mathbf{n}}_k \quad \forall\ 1 \leq k \leq N, \tag{8}$$

where we have $\bar{\mathbf{H}}_k(i,j) = \mathbf{\Lambda}_{ij}(k,k)$, $\bar{\mathbf{y}}_k(i) = \mathbf{y}'_i(k)$, $\bar{\mathbf{x}}_k(j) = \mathbf{x}'_j(k)$ and $\bar{\mathbf{n}}_k(i) = \mathbf{n}'_i(k)$ for $1 \leq i \leq N_r$ and $1 \leq j \leq N_t$.

B. Proposed FDR-BF Scheme

Let $\mathbf{P}_k \in \mathbb{C}^{N_t \times N_{SS}}$ represent the beamforming/precoding matrix chosen for the k^{th} subcarrier. The proposed beamformer is given by

$$\mathbf{P}_k = \mathbf{V}_k(:,[1:N_{SS}])\mathbf{\Phi}_k^{1/2}\mathbf{\Theta}_{N_{SS}}, \tag{9}$$

where $\mathbf{V}_k \in \mathbb{C}^{N_t \times N_t}$ is the right singular matrix of $\bar{\mathbf{H}}_k = \mathbf{U}_k\mathbf{\Sigma}_k\mathbf{V}_k^H$, $\mathbf{\Phi}_k$ is a diagonal matrix that decides the power allocated over parallel channels at the k^{th} subcarrier based on water-filling [18] and $\mathbf{\Theta}_{N_{SS}} \in \mathbb{C}^{N_{SS}\times N_{SS}}$ is the FDR matrix [39]-[41]. Specifically, for the $N_{SS}=2$ case we have $\mathbf{\Theta}_{N_{SS}} = \begin{bmatrix} -0.5257 & -0.8506 \\ -0.8506 & 0.5257 \end{bmatrix}$ [41]. The FDR matrices were originally employed in diagonal STBCs in order to attain full transmit diversity gain [39], [40]. The FDR matrices associated with maximized minimum product distance were designed for $N_{SS} > 1$ and are available in [41]. Note that the authors of [42], [43] also considered a similar precoding scheme as that given by (9), albeit in a different context. Specifically, Svante *et al.* focused on optimizing the bit-loading and $\mathbf{\Theta}_{N_{SS}}$ in [42], where no explicit diversity analysis was provided. By contrast, Amin *et al.* [43] studied the unitary precoding scheme conceived for STBCs in the context of an integer-forcing receiver. In contrast to this, we consider the maximum likelihood (ML) receiver, which only requires $\mathbf{\Theta}_{N_{SS}}$ to have non-zero minimum product distance in order to attain full transmit diversity. Our proposed scheme ensures water-filling based optimal power allocation in contrast to the existing schemes [42], [43], which employ equal-power allocation. Furthermore, in contrast to the STBC based scheme of [43], our transmission scheme does not require coding over time. Lastly, our method of diversity analysis is different from that of the existing literature.

Diversity Analysis: The precoded symbols of the k^{th} subcarrier are given by

$$\bar{\mathbf{x}}_k = \mathbf{P}_k\mathbf{s}_k, \tag{10}$$

$$= \mathbf{V}_k(:,[1:N_{SS}])\mathbf{\Phi}_k^{1/2}\mathbf{\Theta}_{N_{SS}}\mathbf{s}_k, \tag{11}$$

where $\mathbf{s}_k \in \mathbb{C}^{N_{SS}}$, whose elements are drawn from a lattice constellation such as the M-QAM signal set. Let $\mathcal{S}$ represent the set of all possible candidate transmit vectors, whose elements are from an M-QAM signal set. Furthermore, let $\Delta\bar{\mathcal{S}} = \{\mathbf{\Theta}_{N_{SS}}(\mathbf{s}-\mathbf{s}') \mid \mathbf{s},\mathbf{s}' \in \mathcal{S}, \mathbf{s} \neq \mathbf{s}'\}$. Owing to the non-zero minimum product distance of $\mathbf{\Theta}_{N_{SS}}$ [39], we have $\prod_{i=1}^{N_{SS}} |\bar{\mathbf{s}}(i)| > 0, \forall\ \bar{\mathbf{s}} \in \Delta\bar{\mathcal{S}}$. Let $\delta_{min}^2 = \min_{\bar{\mathbf{s}}\in\Delta\bar{\mathcal{S}}} \min_{1\le i\le N_{SS}} |\mathbf{e}_i^T\bar{\mathbf{s}}|^2$, where $\mathbf{e}_i \in \mathbb{R}^{N_{SS}}$ so that $\mathbf{e}_i(j) = \delta(i-j)$. Given a channel realization $\bar{\mathbf{H}}_k$, the pairwise symbol error probability between $\mathbf{s},\mathbf{s}' \in \mathcal{S}$ is given by

$$\mathsf{PEP}(\mathbf{s}\to\mathbf{s}' \mid \bar{\mathbf{H}}_k) = Q\left(\frac{\sqrt{\rho}}{2}\|\bar{\mathbf{H}}_k\mathbf{P}_k(\mathbf{s}-\mathbf{s}')\|\right), \tag{12}$$

$$\le \frac{1}{2}\exp\left(-\frac{\rho}{4}\|\bar{\mathbf{H}}_k\mathbf{P}_k(\mathbf{s}-\mathbf{s}')\|^2\right), \tag{13}$$

where ρ denotes the SNR at each receive antenna and the inequality in (13) follows from the Chernoff bound [44]. Substituting $\mathbf{U}_k\mathbf{\Sigma}_k\mathbf{V}_k^H$ for $\bar{\mathbf{H}}_k$ in (13), we have

$$\mathsf{PEP}(\mathbf{s}\to\mathbf{s}' \mid \bar{\mathbf{H}}_k) \le \frac{1}{2}\exp\left(-\frac{\rho}{4}\|\mathbf{\Sigma}_k\mathbf{V}_k^H\mathbf{P}_k(\mathbf{s}-\mathbf{s}')\|^2\right). \tag{14}$$

Substituting for $\mathbf{P}_k$ from (9), we have

$$\mathsf{PEP}(\mathbf{s}\to\mathbf{s}' \mid \bar{\mathbf{H}}_k) \le \frac{1}{2}\exp\left(-\frac{\rho}{4}\|\mathbf{\Sigma}_k'\mathbf{\Theta}_{N_{SS}}(\mathbf{s}-\mathbf{s}')\|^2\right), \tag{15}$$

$$= \frac{1}{2}\exp\left(-\frac{\rho}{4}\|\mathbf{\Sigma}_k'\bar{\mathbf{s}}\|^2\right), \tag{16}$$

where $\mathbf{\Sigma}_k' = \mathbf{\Sigma}_k(:,[1:N_{SS}])\mathbf{\Phi}_k^{1/2}$ and $\bar{\mathbf{s}} \in \Delta\bar{\mathcal{S}}$. If the singular values of $\bar{\mathbf{H}}_k$ are represented by $\bar{\sigma}_k(i)$, $1 \le i \le N_{SS}$ and the power allocated for the i^{th} parallel channel is $P_k(i)$ so that $P_{tot} = \sum_{i=1}^{N_{SS}} P_k(i)\ \forall k$, we have

$$\mathsf{PEP}(\mathbf{s}\to\mathbf{s}' \mid \bar{\mathbf{H}}_k) \le \frac{1}{2}\exp\left(-\frac{\rho}{4}\sum_{i=1}^{N_{SS}} P_k(i)\bar{\sigma}_k(i)^2|\bar{\mathbf{s}}(i)|^2\right). \tag{17}$$

Due to water-filling power allocation [18], we have $P_k(i) = \left(\mu - \frac{1}{\rho\bar{\sigma}_k(i)^2}\right)_+$, where μ satisfies $\sum_{i=1}^{N_{SS}}\left(\mu - \frac{1}{\rho\bar{\sigma}_k(i)^2}\right)_+ = P_{tot}$. Specifically, the *water level* is set to μ and a power allocation of $\mu - \frac{1}{\rho\bar{\sigma}_k(i)^2}$ is allocated to the i^{th} channel if $\mu - \frac{1}{\rho\bar{\sigma}_k(i)^2} > 0$, else no power is allocated to that channel. For further details on water-filling power allocation, please refer to Sec. 5.3.3 of [18]. At high SNR, we have $\frac{1}{\rho} \to 0$ and hence $P_k(i) \approx \mu \approx P_{tot}/N_{SS}$. Furthermore, we have $\delta_{min}^2\sum_{i=1}^{N_{SS}}\bar{\sigma}_k(i)^2 \le \sum_{i=1}^{N_{SS}}\bar{\sigma}_k(i)^2|\bar{\mathbf{s}}(i)|^2$ for any channel realization. Thus, we have

$$\mathsf{PEP}(\mathbf{s}\to\mathbf{s}' \mid \bar{\mathbf{H}}_k) \le \frac{1}{2}\exp\left(-\frac{\rho P_{tot}\delta_{min}^2}{4N_{SS}}\sum_{i=1}^{N_{SS}}\bar{\sigma}_k(i)^2\right), \tag{18}$$

$$= \frac{1}{2}\exp\left(-\frac{\rho P_{tot}\delta_{min}^2}{4N_{SS}}\|\bar{\mathbf{H}}_k\|_F^2\right), \tag{19}$$

$$= \frac{1}{2}\prod_{i=1}^{N_r}\prod_{j=1}^{N_t}\exp\left(-\frac{\rho}{4}\delta_{min}'^2|\bar{\mathbf{H}}_k(i,j)|^2\right), \tag{20}$$

where $\delta_{min}' = \delta_{min}\sqrt{P_{tot}/N_{SS}}$. For the sake of mathematical tractability, let us assume that the channel between each of the transmit and receive antenna pairs has a fixed number of taps, i.e. $\|\mathbf{h}_{ij}\|_0 = L_a^{(ij)}$. This is a reasonable assumption, since the number of taps and their delays vary slowly compared to their amplitude and phase. Hence, we have $\bar{\mathbf{H}}_k(i,j) = \mathbf{h}_{ij}'(k) \sim \mathcal{CN}\left(0,\sigma_{ij}^2\right)$, where $\sigma_{ij}^2 = \sum_{k=0}^{L_a^{(ij)}-1}\sigma_{p_k^{(ij)}}^2$ so that $p_k^{(ij)}$ $(0 \le k \le L_a^{(ij)}-1)$ represent the baseband channel taps between the i^{th} receive and the j^{th} transmit antennas. Thus, we have

$$\mathsf{PEP}(\mathbf{s}\to\mathbf{s}' \mid \bar{\mathbf{H}}_k) \le \frac{1}{2}\prod_{i=1}^{N_r}\prod_{j=1}^{N_t}\exp\left(-\frac{\rho}{4}(\delta_{min}'\sigma_{ij})^2|\hat{\mathbf{H}}_k(i,j)|^2\right), \tag{21}$$

where $\hat{\mathbf{H}}_k(i,j) = \frac{\bar{\mathbf{H}}_k(i,j)}{\sigma_{ij}} \sim \mathcal{CN}(0,1)$. Since the channels

between the various transmit and receive antenna pairs are statistically independent, we have

$$\mathsf{PEP}(\mathbf{s}\rightarrow\mathbf{s}') \leq \frac{1}{2}\prod_{i=1}^{N_r}\prod_{j=1}^{N_t}\mathbb{E}\left\{\exp\left(-\frac{\rho}{4}(\delta'_{min}\sigma_{ij})^2|\hat{\mathbf{H}}_k(i,j)|^2\right)\right\} \tag{22}$$

$$= \frac{1}{2}\prod_{i=1}^{N_r}\prod_{j=1}^{N_t}\frac{1}{1+\frac{\rho}{4}(\delta'_{min}\sigma_{ij})^2}, \tag{23}$$

$$\approx \frac{1}{2}\left(\prod_{i=1}^{N_r}\prod_{j=1}^{N_t}\frac{4}{(\delta'_{min}\sigma_{ij})^2}\right)\frac{1}{\rho^{N_rN_t}}, \tag{24}$$

where (23) follows from the fact that $|\hat{\mathbf{H}}_k(i,j)|^2$ is an exponential random variable with unit mean and (24) corresponds to the high-SNR approximation, where $\rho \gg 1$. Thus, the upper bound on the probability of symbol error based on the union bound is given by

$$\mathsf{P}_e \leq \frac{1}{|\mathcal{S}|}\sum_{\mathbf{s}\in\mathcal{S}}\sum_{\mathbf{s}\neq\mathbf{s}'\in\mathcal{S}}\mathsf{PEP}(\mathbf{s}\rightarrow\mathbf{s}'), \tag{25}$$

$$\leq \frac{|\mathcal{S}|-1}{2}\left(\prod_{i=1}^{N_r}\prod_{j=1}^{N_t}\frac{4}{(\delta'_{min}\sigma_{ij})^2}\right)\frac{1}{\rho^{N_rN_t}}. \tag{26}$$

From (26) it is evident that the proposed FDR-BF achieves full transmit as well as receive diversity gains. The above theoretical claims are validated through numerical simulations in Section IV.

Capacity Optimality: Assuming that the transmit symbols $\mathbf{s}_k$ are from the Gaussian alphabet, the mutual information [18] of the system in (8) with the proposed precoding is given by

$$MI_k = \log\left[\det(\mathbf{I}_{N_r}+\rho\bar{\mathbf{H}}_k\mathbf{P}_k\mathbf{P}_k^H\bar{\mathbf{H}}_k^H)\right]. \tag{27}$$

Substituting for $\mathbf{P}_k$ from (9) and $\mathbf{U}_k\mathbf{\Sigma}_k\mathbf{V}_k^H$ for $\bar{\mathbf{H}}_k$ in (27), we have

$$MI_k = \log\left[\det(\mathbf{I}_{N_{SS}}+\rho\mathbf{\Sigma}'_k\mathbf{\Theta}_{N_{SS}}\mathbf{\Theta}_{N_{SS}}^H\mathbf{\Sigma}'_k)\right]. \tag{28}$$

Since $\mathbf{\Theta}_{N_{SS}}\mathbf{\Theta}_{N_{SS}}^H = \mathbf{I}_{N_{SS}}$ due to the unitary property of FDR matrices [41], we have

$$MI_k = \log\left[\det(\mathbf{I}_{N_{SS}}+\rho\mathbf{\Sigma}'^2_k)\right], \tag{29}$$

$$= \sum_{i=1}^{N_{SS}}\log[1+\rho P_k(i)\bar{\sigma}_k(i)^2], \tag{30}$$

which is essentially the capacity of the system in (8). Thus, the proposed scheme is deemed to be *information-lossless*, i.e. the maximum attainable mutual information of the proposed system is the same as the system's capacity.

Impact of Limited Feedback: In the above diversity analysis, we assumed that the transmitter has perfect CSI. In practice, this will not be the case owing to the limited number of bits available in the feedback channel. Explicitly, the transmitter would have a quantized channel $\bar{\mathbf{H}}_k^q$ instead of $\bar{\mathbf{H}}_k$ so that $\bar{\mathbf{H}}_k^q = \bar{\mathbf{H}}_k + \Delta\bar{\mathbf{H}}_k$, where $\Delta\bar{\mathbf{H}}_k$ is due to the quantization noise. Considering the proposed TDQ, let the quantized version of the time-domain channel $\mathbf{h}_{ij}$ be denoted by $\mathbf{h}_{ij}^q$. The instantaneous distortion due to the quantization error is given by $\|\mathbf{h}_{ij}-\mathbf{h}_{ij}^q\|^2$. The corresponding frequency-domain distortion is given by $\|\mathbf{h}'_{ij} - \mathbf{h}'^q_{ij}\|^2 = \|\mathbf{F}_N(\mathbf{h}_{ij}-\mathbf{h}_{ij}^q)\|^2 = N\|\mathbf{h}_{ij}-\mathbf{h}_{ij}^q\|^2$. Thus, we have $\mathbb{E}[\|\mathbf{h}'_{ij}-\mathbf{h}'^q_{ij}\|^2] = N\mathbb{E}[\|\mathbf{h}_{ij}-\mathbf{h}_{ij}^q\|^2]$. When employing Algorithm 1 using the optimal number of quantization bits, we have $D_t = \mathbb{E}[\|\mathbf{h}_{ij}-\mathbf{h}_{ij}^q\|^2] \lesssim \sum_{i=0}^{L_q-1}\frac{\Delta_i^2}{12} = \sum_{i=0}^{L_q-1}\frac{B_i\sigma_i^2}{3\log e}2^{-2\bar{B}_i}$ [37]. Thus, the average distortion associated with each of the taps reduces exponentially with the number of quantization bits $\bar{B}_i$, which is also evident from Fig. 2. Since $\|\Delta\bar{\mathbf{H}}_k\|^2 \propto \sum_{i=1}^{N_r}\sum_{j=1}^{N_t}\|\mathbf{h}'_{ij}-\mathbf{h}'^q_{ij}\|^2$, we can expect $\|\Delta\bar{\mathbf{H}}_k\|^2$ to be negligible, when the number of bits employed for quantizing each of the links between the transmit and receive antenna pair is sufficiently high. In the next section, we show that about 30 quantization bits, which corresponds to a distortion level of $D_t = 10^{-2}$ (refer Fig. 2), would be sufficient to attain the same performance as that attained by having perfect CSI.

IV. Simulation Results and Discussions

Simulation Scenario: In all our simulations, we assume $N_{CP} = 32$ and $N = 64$ subcarriers. The BER performance of all the schemes is evaluated by assuming perfect CSI and an ML detector at the receiver. For evaluating a BER of 10^{-t}, we have employed at least 10^{t+1} bits in all our simulations. All the MIMO schemes assume $N_t = N_r = N_{SS} = 2$. The MIMO scheme employing SVD based BF [18] is referred to as MIMO-SVD. The MIMO scheme employing strongest Eigenmode transmission is referred to as EMT. The single-input multiple-output (SIMO) system corresponds to a system having $N_t = 1$ and $N_r = 2$. Each transmitted OFDM symbol is appropriately normalized to ensure that the average signal energy is the same across all the schemes considered in the paper. For the ease of presentation, we use the following definition of datarate:

$$\mathsf{rate} = \frac{N_{SS}\times\text{No. of information bits per OFDM stream}}{N},$$

which ignores the overhead due to CP. Owing to the limited space, we consider only the two extreme elevation angles in our simulation studies, i.e. $\Psi \in \{30^o, 7.5^o\}$. The performance curves associated with the other two elevation angles are observed to fall between the curves associated with the above two angles and are not included. For simulating a coded system, we consider a convolutional encoder associated with the industry-standard octal generator polynomials, $\mathsf{g}_0 = 133_8$ and $\mathsf{g}_1 = 171_8$ of coding rate 1/2 as specified in 18.3.5.6 of the 802.11n/ac standard [32]. The encoded bits are interleaved using a block-interleaver of appropriate length, which depends on the operating datarate. At the receiver, the ML decoded bits are deinterleaved and passed on to the Viterbi decoder for obtaining the information bits.

A. Comparison with the Existing Schemes

Assuming perfect CSIT, let us now compare the BER performance of the proposed FDR-BF to that of the classic SIMO, MIMO-VBLAST, MIMO-SVD and GMD [20] schemes. Fig. 3 portrays the BER performance of the aforementioned schemes

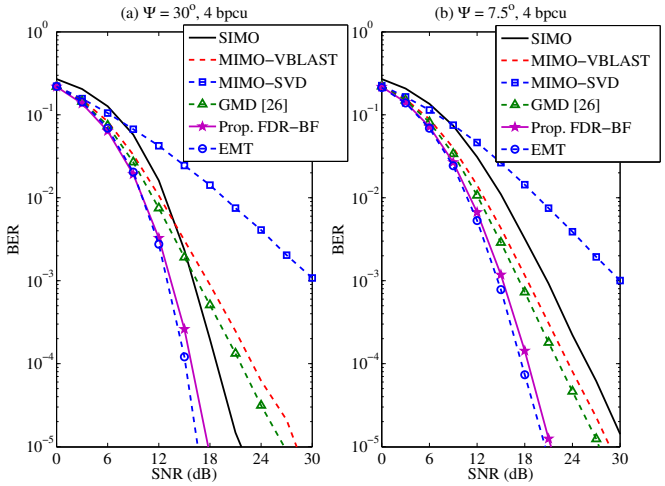

Fig. 3. Comparison of the BER performance of the proposed FDR-BF scheme with that of SIMO, MIMO, MIMO-SVD, EMT and GMD [20] schemes. All the systems are assumed to be operating at a rate of 4 bpcu. Plot (a) corresponds to the elevation angle of $\Psi = 30^o$, whereas Plot (b) corresponds to that of $\Psi = 7.5^o$.

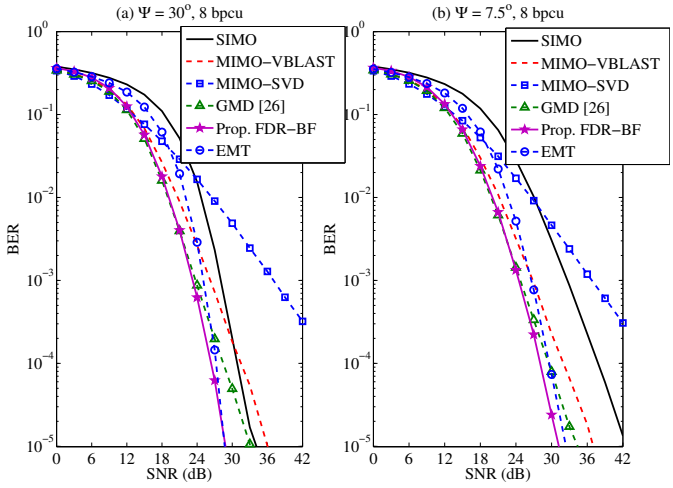

Fig. 4. Comparison of the BER performance of the proposed FDR-BF scheme with that of SIMO, MIMO, MIMO-SVD, EMT and GMD [20] schemes. All the systems are assumed to be operating at a rate of 8 bpcu. Plot (a) corresponds to the elevation angle of $\Psi = 30^o$, whereas Plot (b) corresponds to that of $\Psi = 7.5^o$.

operating at a datarate of 4 bpcu and elevation angles of $\Psi \in \{30^o, 7.5^o\}$. Specifically, Fig. 3(a) corresponds to the elevation angle of $\Psi = 30^o$, whereas Fig. 3(b) corresponds to that of $\Psi = 7.5^o$. The following observations can be made from Fig. 3:

1) The MIMO-SVD scheme performs poorly compared to the other schemes owing to the unequal SNR over the parallel subchannels. The effective BER performance at high SNR is dictated by the subchannel associated with the lowest singular value.
2) The SIMO system performs better than the MIMO-VBLAST and GMD schemes at $\Psi = 30^o$ and worse when $\Psi = 7.5^o$. This is due to the relatively shorter delay spread at $\Psi = 30^o$, which enables the ML detector to attain higher power gain across all the subcarriers. When the delay spread is longer as in the case of $\Psi = 7.5^o$, the chances of some subcarriers being in deep fade would be high.
3) The GMD scheme performs better than the MIMO-VBLAST as well as the MIMO-SVD schemes, owing to the beamforming gain as well as due to having equal SNRs across all the parallel subchannels.
4) The proposed FDR-BF scheme outperforms the other schemes at both the elevation angles. Specifically, at a BER of 10^{-5} the proposed scheme provides an SNR gain of about 3dB compared to the SIMO system at $\Psi = 30^o$ and about 6dB compared to the GMD scheme at $\Psi = 7.5^o$.
5) The performance of the FDR-BF scheme is comparable to that of EMT when operating at 4 bpcu, while the proposed scheme outperforms the EMT at 8 bpcu as evident from Fig. 4.

Figure 4 provides the BER performance of the aforementioned schemes operating at a datarate of 8 bpcu. Similar observations to 1)-4) hold for this case as well. It can be observed from Fig. 3 and Fig. 4 that both the proposed as well as the existing schemes suffer from performance loss, when the elevation angle drops. Fig. 5 provides the BER performance of the proposed scheme operating at various rates and elevation angles. It is evident from Fig. 5 that lower elevations result in performance degradation compared to higher elevation angles at all datarates. Specifically, there is a performance degradation of 3dB at a datarate of 4bpcu and about 2dB in case of 6 and 8bpcu.

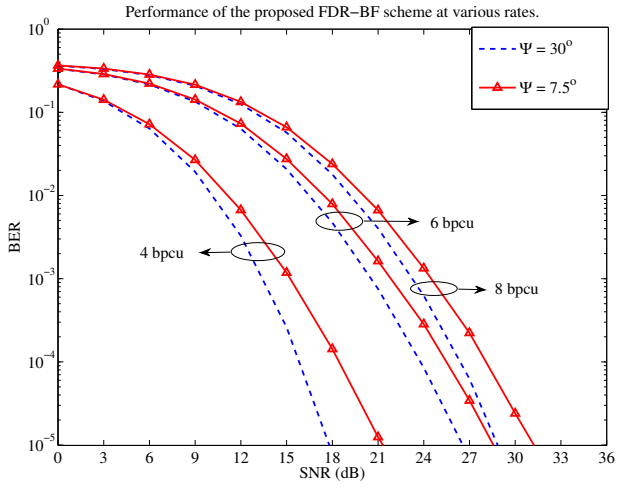

Fig. 5. BER performance of the proposed FDR-BF scheme at various rates and elevation angles.

Remark 1: In case of multi-user beamforming, where multiple users are located at different elevation angles with respect to the aerial transmitter, the elevation angle should be taken into account in addition to the SNR of each user in order to decide the modulation and coding scheme for each user.

B. Proposed TDQ vs. FDQ of 802.11 [32]

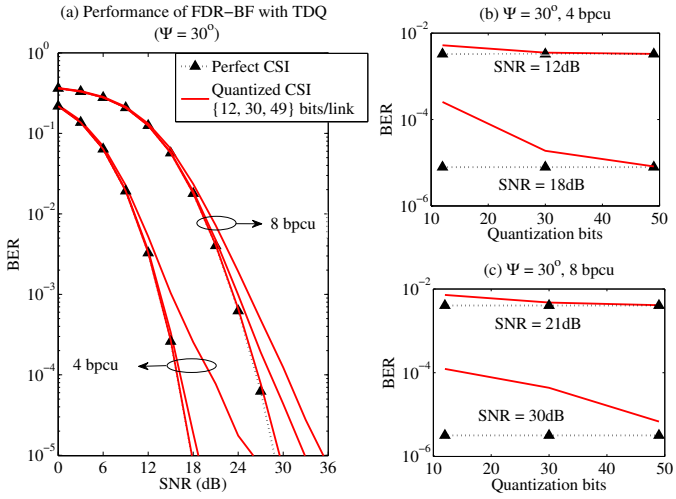

Fig. 6. Comparison of the BER performance of the proposed FDR-BF scheme operating at 4 and 8 bpcu with the aid of perfect and quantized CSI at the transmitter. The aerial transmitter is assumed to be at an elevation of $\Psi = 30^o$. Plot (a) depicts the variation in BER as a function of SNR, whereas Plot (b) and Plot (c) depict the variation in BER as a function of the number of quantization bits employed in TDQ.

Let us compare the BER performance of the proposed scheme operating both with perfect and with quantized CSI. The quantized CSI is obtained by employing the proposed TDQ that employs the optimal number of quantization bits given in (2). For the three distortion levels $\{10^{-1}, 10^{-2}, 10^{-3}\}$, the optimal number of quantization bits are $\{12, 30, 49\}$ for $\Psi = 30^o$ and $\{14, 30, 51\}$ for $\Psi = 7.5^o$. Figure 6 compares the BER performance of the proposed FDR-BF scheme operating both with perfect and with quantized CSI at $\Psi = 30^o$. It is evident from Fig. 6(a) that the proposed scheme operating with a CSI quantized to 30 bits attains essentially the same performance as that of the perfect CSI at low to moderate SNRs. Fig. 6(b) and Fig.6(c) depict the variation in the BER as a function of the number of quantization bits employed in TDQ for the two datarates of 4 and 8 bpcu, respectively.

Figure 7 provides the BER performance of the proposed scheme operating both with perfect and with quantized CSI for $\Psi = 7.5^o$. Similar observations to those of Fig. 6 hold for this case as well.

Let us compare the BER performance of the proposed scheme operating with quantized CSI obtained based on the FDQ of 802.11. We assume an FDQ employing $N_b = 4$ bits [32], which corresponds to the lowest number of quantization bits supported by the standard. Note that $N_b = 4$ corresponds to $N_{FDQ} = 1820$ bits. Figure 8 provides the BER performance of the proposed FDR-BF scheme operating at various rates both with perfect and with FDQ based CSI for $\Psi = 30^o$ and $\Psi = 7.5^o$. It is evident from both Fig. 8(a) and Fig. 8(b) that the BER performance of the proposed scheme operating with quantized CSI is essentially the same as that of perfect CSI. Thus, the minimum number of quantization bits supported

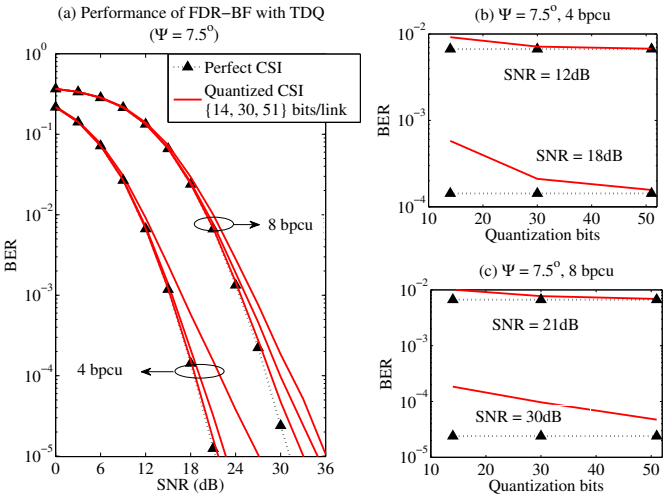

Fig. 7. Comparison of the BER performance of the proposed FDR-BF scheme operating at 4 and 8 bpcu with the aid of perfect and quantized CSI at the transmitter. The aerial transmitter is assumed to be at an elevation of $\Psi = 7.5^o$. Plot (a) depicts the variation in BER as a function of SNR, whereas Plot (b) and Plot (c) depict the variation in BER as a function of the number of quantization bits employed in TDQ.

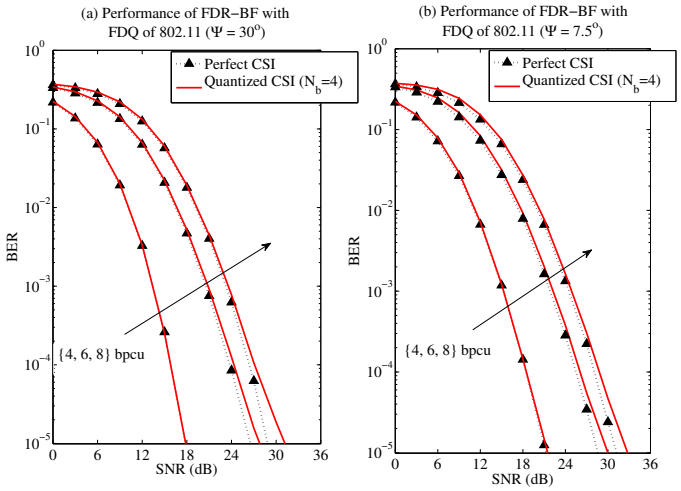

Fig. 8. Comparison of the BER performance of the proposed FDR-BF scheme operating at various rates with the aid of perfect CSI and quantized CSI obtained based on FDQ of 802.11 [32]. The FDQ is assumed to employ $N_b = 4$ bits, which corresponds to $N_{FDQ} = 1820$ bits. Plot (a) corresponds to the elevation angle of $\Psi = 30^o$, whereas Plot (b) corresponds to that of $\Psi = 7.5^o$.

by the standard would be sufficient to attain the optimal performance and hence the higher quantization resolutions that correspond to $N_b \in \{5, 6, 8\}$ [32] may not be required in the aerial communication scenario. This is mainly due to the sparsity of the A2G multipath channel, which renders the frequency-domain channel somewhat flat compared to that of the more rich indoor scattering environment.

Remark 2: The proposed scheme operating with the aid of TDQ attains nearly the same optimal performance as that attained by employing FDQ of 802.11. Considering the fact

that the number of quantization bits required in case of TDQ is far lesser than that of FDQ, it would be beneficial to relook at the medium access control (MAC)-level beamforming training protocol of the existing 802.11 standard, which may help in significantly reducing the overhead involved in conveying the quantized CSI.

C. Coded BER Performance

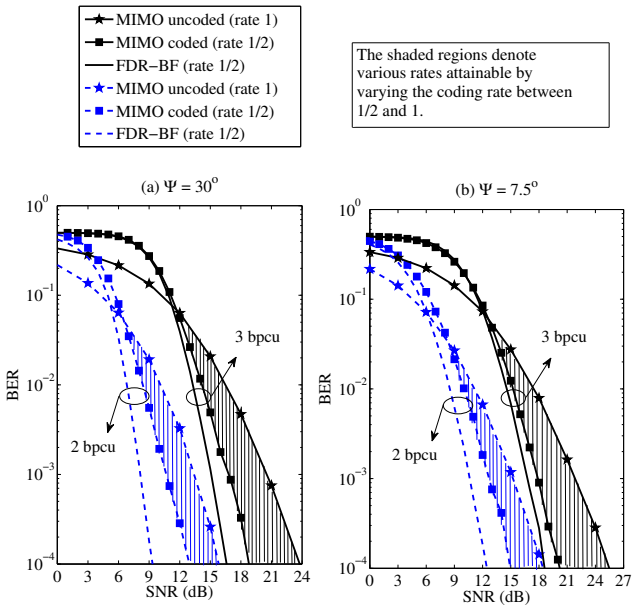

Fig. 9. Comparison of the coded BER performance of the proposed FDR-BF scheme with that of the MIMO scheme. The BER performance of the uncoded MIMO system is also provided for comparison. Plot (a) corresponds to the elevation angle of $\Psi = 30^o$, whereas Plot (b) corresponds to that of $\Psi = 7.5^o$.

The coded BER performance of the proposed as well as that of the MIMO system are provided for the datarates of 2 and 3 bpcu in Fig. 9, where both the transmitter as well as the receiver are assumed to have perfect CSI. The performance of the uncoded MIMO system is also provided in order to show the potentially attainable BER performance by varying the coding rate. This corresponds to the shaded regions in both Fig. 9(a) and Fig. 9(b). It can be seen from Fig. 9(a) and Fig. 9(b) that when operating at 2 bpcu, the proposed scheme provides an SNR gain of about 4dB with respect to the coded MIMO system at $\Psi = 30^o$ and about 2.5dB at $\Psi = 7.5^o$. These SNR gains enable us to extend the signal range and hence the coverage area. When operating at 3 bpcu, the SNR gain attained by the proposed scheme with respect to the MIMO system is about 2.5dB at $\Psi = 30^o$ and about 2dB at $\Psi = 7.5^o$.

Figure 10 compares the coded BER performance of the proposed scheme operating at various rates and employing: (a) perfect CSI, (b) CSI obtained based on TDQ with 30 bits/link and (c) CSI obtained based on FDQ of 802.11 with $N_b = 4$. Figure 10(a) corresponds to an elevation angle of $\Psi = 30^o$, while Figure 10(b) corresponds to an elevation of $\Psi = 7.5^o$. It

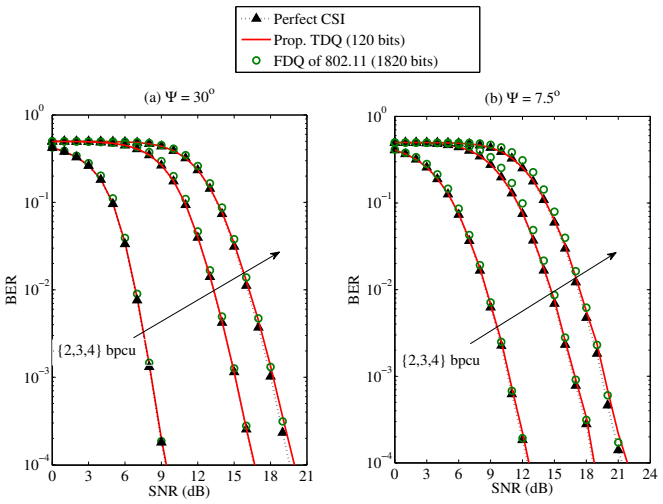

Fig. 10. Comparison of the coded BER performance of the proposed FDR-BF scheme operating with the aid of perfect CSI and that obtained based on the proposed TDQ as well as the FDQ of 802.11 [32]. The three rates of 2, 3 and 4 bpcu are attained by employing 4-QAM, 8-QAM, and 16-QAM in conjunction with a rate-1/2 convolutional code, respectively. Plot (a) corresponds to the elevation angle of $\Psi = 30^o$, whereas Plot (b) corresponds to that of $\Psi = 7.5^o$.

is evident from Figure 10(a) and Figure 10(b) that the proposed scheme operating with quantized CSI obtained from TDQ or FDQ of 802.11 attains the same performance as that of the perfect CSI. Thus, the proposed TDQ which requires only a few feedback bits is an attractive solution compared to the existing FDQ of 802.11 standard.

V. Conclusions and Future Directions

We have provided a statistical model for the A2G multipath channel, which is beneficial for the design and analysis of aerial communication systems deployed as LAPs. The proposed A2G channel model was utilized for designing a time-domain quantizer, which was shown to require much less quantization bits than the frequency-domain quantizer employed in the 802.11n/ac standard. Furthermore, a beamforming aided full-diversity scheme was proposed with the aid of full-diversity rotation matrices. The symbol error probability of the proposed scheme was evaluated analytically and the attainable diversity order was shown to be $N_t N_r$. Furthermore, the proposed scheme was shown to be *information-lossless*. It was shown through numerical simulations that the proposed scheme outperforms several existing schemes when operating at various elevation angles. Furthermore, the BER performance of the proposed scheme was studied under quantized CSI obtained based on the proposed TDQ as well as the FDQ of 802.11. It was observed in both coded as well as uncoded scenarios that the BER performance attained by the proposed scheme employing the TDQ is the same as that of perfect CSI, despite using far less quantization bits than that required by the FDQ of 802.11n/ac.

In all our studies, we have fixed the length of CP to be $N_{CP} = 32$, which caters for the maximum multipath delay of $1.6\mu s$. This can be reduced, especially at higher elevations,

where the RMS delay spread is small. Note that the 802.11n/ac supports two guard intervals: $0.4\mu s$ and $0.8\mu s$. These would be too large for higher elevations, where the RMS delay spread is only of the order of 10's of nanoseconds. It would be beneficial to study the impact of having lower CP lengths on the performance at various elevation angles. The 802.11n/ac employs cyclic shift delays (CSD) [45] across multiple streams in order to exploit multipath delay diversity as well as to avoid undesirable beamforming effects when transmitting the same signal across all the transmit antennas. This would be only beneficial in rich multipath scattering. In case of sparse multipath scattering as in the case of A2G channel, it would be highly inefficient [46]. Thus, it is important to study the impact of CSD on the performance at various elevation angles.

REFERENCES

[1] S. Chandrasekharan et al., "Designing and implementing future aerial communication networks," *IEEE Commun. Magazine*, vol. 54, no. 5, pp. 26-34, May 2016.

[2] Y. Zeng, R. Zhang and T. J. Lim, "Wireless communications with unmanned aerial vehicles: opportunities and challenges," *IEEE Commun. Magazine*, vol. 54, no. 5, pp. 36-42, May 2016.

[3] S. Hayat, E. Yanmaz and R. Muzaffar, "Survey on Unmanned aerial vehicle networks for civil applications: A communications viewpoint," *IEEE Communications Surveys & Tutorials*, vol. 18, no. 4, pp. 2624-2661, Fourthquarter 2016.

[4] J-J. Wang, C-X. Jiang, Z. Han, Y. Ren, R. G. Maunder, and L. Hanzo, "Taking drones to the next level: Cooperative distributed unmanned-aerial-vehicular networks for small and mini drones," *IEEE Veh. Technol. Mag.*, vol. 12, no. 3, pp 73 - 82, 2017.

[5] A. Al-Hourani, S. Kandeepan and S. Lardner, "Optimal LAP altitude for maximum coverage," *IEEE Wireless Commun. Lett.*, vol. 3, no. 6, pp. 569-572, Dec. 2014.

[6] A. Vilhar, A. Hrovat, T. Javornik and M. Mohorcic, "Experimental analysis of wireless temporary networks deployed by low altitude platforms," *IEEE 18th International Workshop on Computer Aided Modeling and Design of Communication Links and Networks (CAMAD), Berlin*, pp. 238-242, 2013.

[7] I. Bucaille, S. Hethuin, A. Munari, R. Hermenier, T. Rasheed and S. Allsopp, "Rapidly deployable network for tactical applications: Aerial base station with opportunistic links for unattended and temporary events ABSOLUTE example," *in Proc. MILCOM 2013 - 2013 IEEE Military Communications Conference, San Diego, CA*, pp. 1116-1120, 2013.

[8] J-K. Zhang, S. Chen, R. G. Maunder, R. Zhang and L. Hanzo, "Adaptive coding and modulation for large-scale antenna array-based aeronautical communications in the presence of co-channel interference," *IEEE Trans. Wireless Commun.*, vol. 17, no. 2, pp. 1343 - 1357, 2018.

[9] Z. Wu, H. Kumar and A. Davari, "Performance evaluation of OFDM transmission in UAV wireless communication," *in Proc. Thirty-Seventh Southeastern Symposium on System Theory (SSST '05)*, pp. 6-10, 2005.

[10] E. Yanmaz, R. Kuschnig and C. Bettstetter, "Achieving air-ground communications in 802.11 networks with three-dimensional aerial mobility," *2013 Proceedings IEEE INFOCOM, Turin*, pp. 120-124, 2013.

[11] M. Asadpour, D. Giustiniano, and K. A. Hummel, "From ground to aerial communication: Dissecting WLAN 802.11n for the drones," *in Proc. ACM Int. Workshop Wireless Netw. Testbeds Experimental Eval. Characterization (WiNTECH), Miami, FL, USA*, pp. 25-32, 2013.

[12] E. Yanmaz, S. Hayat, J. Scherer and C. Bettstetter, "Experimental performance analysis of two-hop aerial 802.11 networks," *2014 IEEE Wireless Communications and Networking Conference (WCNC), Istanbul*, pp. 3118-3123, 2014.

[13] S. Hayat, E. Yanmaz and C. Bettstetter, "Experimental analysis of multipoint-to-point UAV communications with IEEE 802.11n and 802.11ac," *2015 IEEE 26th Annual International Symposium on Personal, Indoor, and Mobile Radio Communications (PIMRC), Hong Kong*, pp. 1991-1996, 2015.

[14] A. Guillen-Perez, R. Sanchez-Iborra, M. D. Cano, J. C. Sanchez-Aarnoutse and J. Garcia-Haro, "WiFi networks on drones," *2016 ITU Kaleidoscope: ICTs for a Sustainable World (ITU WT), Bangkok*, pp. 1-8, 2016.

[15] H. Jamal and D. W. Matolak, "Multicarrier air to ground MIMO communication system performance," *in Proc. 2016 IEEE 84th Vehicular Technology Conference (VTC-Fall), Montreal, QC*, pp. 1-5, 2016.

[16] C. Zhang and Y. Hui, "Broadband air-to-ground communications with adaptive MIMO datalinks,"*in Proc. 2011 IEEE/AIAA 30th Digital Avionics Systems Conference, Seattle, WA*, pp. 4D4-1-4D4-10, 2011.

[17] J. Chen et al., "Long-range and broadband aerial communication using directional antennas (ACDA): Design and implementation," *IEEE Trans. Veh. Technol.*, vol. 66, no. 12, pp. 10793-10805, Dec. 2017.

[18] D. Tse and P. Viswanath, Fundamentals of Wireless Communications. Cambridge, U.K.: Cambridge Univ. Press, 2005.

[19] Y. Jiang, W. Hager, and J. Li, "The geometric mean decomposition," *Linear Algebra and Its Applications*, vol. 396, pp. 373-384, Feb. 2005.

[20] Y. Jiang, J. Li and W. W. Hager, "Joint transceiver design for MIMO communications using geometric mean decomposition," *IEEE Trans. Signal Process.*, vol. 53, no. 10, pp. 3791-3803, Oct. 2005.

[21] Y. Jiang, J. Li and W. W. Hager, "Uniform channel decomposition for MIMO communications," *IEEE Trans. Signal Process.*, vol. 53, no. 11, pp. 4283-4294, Nov. 2005.

[22] S. Zhou and G. B. Giannakis, "Optimal transmitter eigen-beamforming and space-time block coding based on channel mean feedback," *IEEE Trans. Signal Process.*, vol. 50, no. 10, pp. 2599-2613, Oct. 2002.

[23] Z. Lei, F. P. S. Chin and Ying-Chang Liang, "Combined beamforming with space-time block coding for wireless downlink transmission," *in Proc. IEEE 56th Vehicular Technology Conference*, vol.4, pp. 2145-2148, 2002.

[24] S. Ekbatani and H. Jafarkhani, "Combining beamforming and space-time coding using quantized feedback," *IEEE Trans. Wireless Commun.*, vol. 7, no. 3, pp. 898-908, Mar. 2008.

[25] S. Ekbatani and H. Jafarkhani, "Combining beamforming and space-time coding using noisy quantized feedback," *IEEE Trans. Commun.*, vol. 57, no. 5, pp. 1280-1286, May 2009.

[26] H. Wang, Y. Li, X. G. Xia and S. Liu, "Unitary and non-unitary precoders for a limited feedback precoded OSTBC system," *IEEE Trans. Veh. Technol.*, vol. 62, no. 4, pp. 1646-1654, May 2013.

[27] W. G. Newhall et al., "Wideband air-to-ground radio channel measurements using an antenna array at 2 GHz for low-altitude operations," *IEEE Military Communications Conference (MILCOM 2003.)*, vol. 2, pp. 1422-1427, 2003.

[28] T. J. Willink, C. C. Squires, G. W. K. Colman and M. T. Muccio, "Measurement and characterization of low-altitude air-to-ground MIMO channels," *IEEE Trans. Veh. Technol.*, vol. 65, no. 4, pp. 2637-2648, April 2016.

[29] D. W. Matolak and R. Sun, "Air-ground channel characterization for unmanned aircraft systems-Part III: The suburban and near-urban environments," *IEEE Trans. Veh. Technol.*, vol. 66, no. 8, pp. 6607-6618, Aug. 2017.

[30] X. Cai et al., "Low altitude UAV propagation channel modelling," *2017 11th European Conference on Antennas and Propagation (EUCAP), Paris*, pp. 1443-1447, 2017.

[31] J. B. Andersen, T. S. Rappaport and S. Yoshida, "Propagation measurements and models for wireless communications channels," *IEEE Commun. Mag.*, vol. 33, no. 1, pp. 42-49, Jan 1995.

[32] Part 11: Wireless LAN Medium Access Control (MAC) and Physical Layer (PHY) Specifications, IEEE Standard 802.11, March 2012.

[33] K. K. Mukkavilli, A. Sabharwal, E. Erkip, and B. Aazhang, "On beamforming with finite rate feedback in multiple-antenna systems," *IEEE Trans. Inf. Theory*, vol. 49, no. 10, pp. 2562-2579, Oct. 2003

[34] V. Raghavan, R. W. Heath Jr., and A. M. Sayeed, "Systematic codebook designs for quantized beamforming in correlated MIMO channels," *IEEE J. Sel. Areas Commun.*, vol. 25, no. 7, pp 1298-1310, Sep. 2007.

[35] H. Shirani-Mehr and G. Caire, "Channel state feedback schemes for multiuser MIMO-OFDM downlink," *IEEE Trans. Commun.*, vol. 57, no. 9, pp. 2713-2723, Sept. 2009.

[36] Y. S. Jeon, H. M. Kim, Y. S. Cho and G. H. Im, "Time-domain differential feedback for massive MISO-OFDM systems in correlated channels," *IEEE Trans. Commun.*, vol. 64, no. 2, pp. 630-642, Feb. 2016.

[37] R. M. Gray and D. L. Neuhoff, "Quantization," *IEEE Trans. Inf. Theory*, vol. 44, no. 6, pp. 2325-2383, Oct 1998.

[38] T. M. Cover and J. A. Thomas, "Elements of Information Theory". New York: Wiley, 1991.

[39] M. O. Damen, K. Abed-Meriam, and J.-C. Belfiore, "Diagonal algebraic space-time block codes," *IEEE Trans. Inf. Theory*, vol. 48, no. 3, pp. 628-636, Mar. 2002.

[40] E. Bayer-Fluckiger, F. Oggier, and E. Viterbo, "New algebraic constructions of rotated Zn-lattice constellations for the Rayleigh fading channel," *IEEE Trans. Inf. Theory*, vol. 50, no. 4, pp. 702-714, Apr.2004.
[41] E. Viterbo. Full diversity rotations. Available: http://www.ecse.monash.edu.au/staff/eviterbo/rotations/rotations.html
[42] S. Bergman and B. Bjorn, "Lattice-based linear precoding for MIMO channels with transmitter CSI," *IEEE Trans. Signal Process.*, vol. 56, no. 7, pp. 2902-2914, July 2008.
[43] A. Sakzad and E. Viterbo, "Full diversity unitary precoded integer-forcing," *IEEE Trans. Wireless Commun.*, vol. 14, no. 8, pp. 4316-4327, Aug. 2015.
[44] S. H. Chang, P. C. Cosman and L. B. Milstein, "Chernoff-type bounds for the gaussian error function," *IEEE Trans. Commun.*, vol. 59, no. 11, pp. 2939-2944, Nov. 2011.
[45] A. Dammann and S. Kaiser, "Transmit/receive-antenna diversity techniques for OFDM systems," *European Trans. Telecommun.*, vol. 13, no. 5, pp. 531-538, 2002.
[46] A. Dammann, R. Raulefs and S. Plass, "Soft cyclic delay diversity and its performance for DVB-T in ricean channels," *in Proc. IEEE GLOBECOM 2007 - IEEE Global Telecommunications Conference, Washington, DC*, pp. 4210-4214, 2007.